

Strain gauging for accurate determination of K and G in impact tests

J. P. DEAR, J. H. MacGILLIVRAY

Department of Mechanical Engineering, Imperial College of Science, Technology and Medicine, Exhibition Road, London SW7 2AZ, UK

Impact testing of materials is becoming increasingly important as a wide range of new materials are being developed for demanding high loading-rate working conditions. Charpy pendulum and many other impact-testing machines are being better instrumented to provide more information about the forces acting on a specimen up to and during fracture. Mostly, the force sensors are near the points of contact on the striker or the support and these can provide well for recording the overall forces acting on the specimen to be monitored. Of increasing interest is the distribution of stress and strain within the specimen during the initiation and propagation of fracture. This paper reports research using on-specimen strain-gauge sensors for impact testing of non-metallic specimens. Comparisons are made between force–time traces from sensors on the specimen and those located on the striker. Observations are made as to how the stresses relate to the fast crack in the core of the material specimen and those acting on the surface of the material about the crack, and also those acting on the plastic hinge formed on the compression side of the specimen. Optical and scanning electron microscopic studies are made of the crack surfaces and high-speed photography is used to observe the crack propagation in specimens with and without side-grooves to guide the crack and increase constraint.

1. Introduction

Impact testing is extensively used in research and production of materials and their manufacture into an increasingly wide range of products. With advances in metallic and non-metallic materials that provide for lighter weight, greater strength, higher working temperatures, easier fabrication, lower cost and many other improved attributes, so the types of impact testing required varies greatly. For many materials and products, the trend is towards higher rates of testing together with the need for more precise impact measurements. Advances in impact-tester design are many and some important steps forward have been made to provide better instrumentation of striker and support points [1–3]. This is in order to record more reliable force–time and crack-length measurements and process them to generate a variety of useful derived data, such as critical stress intensity factor (K_c) and critical strain energy release rate (G_c) [4, 5]. A problem in some cases can be that such sensors only see the overall forces acting on the specimen at its contact points with the striker and supports.

However, for a lot of testing, this can be all that is required and also such testing can be validated by more detailed testing of representative samples of materials and products. For research into new materials and their fabrication into what can be complex structures, impact test arrangements can, of course, be correspondingly complex. Mostly, this paper reports work of the kind that would be needed to validate

impact testers having sensors only at striker or support contact points. Also covered is some testing that would be needed for research in more depth on the impact properties of materials. This is to find ways of positioning sensors on the specimens to be tested to study the changing levels of strain in the specimen during rapid loading to initiate and propagate a crack. The work presented is part of wider research into impact properties of materials [6–13] and this paper concentrates on three-point bend impact testing of polymer materials.

As with most materials, the strain at the surface of a polymer specimen can vary from that in the central core. Also, fast running cracks will tend to be initiated in the central bulk of a specimen whereas surface material has the propensity to tear. With three-point bending of a specimen then, of course, one part of the specimen will be compressed and the other put in tension and the neutral line will change its position as the specimen cracks. Often, it is very difficult to achieve fast bending rates without inducing transient oscillations. In the case of impact testers there can also be bounce at the striker and loss of contact at the supports [14–17].

Another interesting point is that few materials if any have a simple change of fracture behaviour when moving from static to dynamic loading rates. Apart from the inherent response time of the specimen necessary to generate crack initiation and propagation processes, a specimen can fail in different ways. For

example, for relatively slow loading rates of polyethylene, there can be considerable crack tip blunting, it is not until a critical loading rate is reached that fast brittle crack growth in the core of the material is initiated [18]. It follows that care is needed when trying to relate static loading conditions with those of higher dynamic loading rates. Also, such relationships vary whether considering static loading and brittle cracking of the core of the material or the ductile tearing of the surface material about the fast brittle crack. These factors are not explored in this paper but they are part of the interest of the overall research programme.

Finding the best on-specimen sensor locations needs to have regard for these factors and care is needed to place sensors to avoid interference with the natural response of the specimen. Attachment should not modify the properties of the material by aggressive abrasion, chemical cleaning, very active bonding agents and such processes. However, a secure attachment of sensors is needed and some polymers do not have easy-to-bond surfaces. The main objectives of the work presented in this paper were as follows:

1. to find sensors suitable for attaching to polymer materials and to develop a reliable attachment technique. This is preferably to be one that could easily be done within test laboratory areas;
2. to monitor the changing strains in different parts of the polymer specimens as induced by a drop-weight instrumented three-point bend tester so that comparisons may be made between overall loads applied to the specimen and the strains created in different parts of the specimen;
3. to study the effects of tear lips on the sides of the fracture surface and how these affected the loading on the crack, as seen by monitoring the strain in the specimen near to the crack tip;
4. to observe the effects upon the strain induced in several parts of a specimen when subjected to different striker impact velocities and changes in the temperature of the specimen being tested.

2. Experimental details

2.1. Experimental equipment

The three-point bend impact tester selected for this study was a drop-weight machine with a falling mass of 65 kg. At a velocity of 5 m s^{-1} this gave an available energy of $\sim 0.8 \text{ kJ}$ to allow specimens of dimensions $12 \text{ mm} \times 40 \text{ mm} \times 200 \text{ mm}$ to be tested. Using this size of specimen meant that the 1.5 mm length strain gauges were relatively small making it easier to explore more precisely the strain on different parts of the specimen. Also, the tested specimens were approximately the same size as metal specimens studied and reported elsewhere [6, 7]. Finally, the failure of polymer specimens of this size was of particular interest to the researchers. The selected strain gauges were a self-temperature compensated constantan foil with polyimide backing. They were connected in a three-wire 1/4 bridge configuration to amplifiers with a frequency response of 1 dB and 200 kHz and the amplifier outputs were monitored on a 20 MHz digital storage

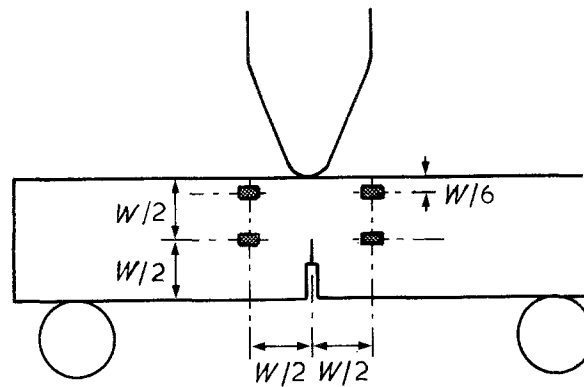


Figure 1 Schematic diagram of three-point bend test configuration showing location sites of on-specimen strain gauges.

scope. The sensor on the striker used a full bridge of semiconductor strain gauges and was monitored in a similar way as the on-specimen gauges. The general arrangement is illustrated in Fig. 1 which shows the specimen resting on two rollers of diameter 25 mm, the tip radius of the striker being 10 mm.

2.2. Specimen preparation

The dimensions of the specimens were thickness, B (12 mm), width, W (40 mm) and overall length, L (200 mm), with a span, S (160 mm) and a pre-notch of depth 15 mm; at the root of the notch, a razor-sharp pre-crack of depth 5 mm was made immediately before the test. The surface of the specimen where the strain gauges were to be attached was carefully abraded and cleaned taking care not to leave any deep grooves or residue of cleaning materials. An effective and readily available cleaning agent proved to be acetone degreaser. The attachment site was then heat-treated just before bonding of the gauge to the surface with a cyanoacrylate adhesive. A thin glue-line was achieved by using carefully metered amounts of adhesive and quickly applying a firm steady pressure to the bond.

Particular care had to be taken with polyethylene and such materials, whereas there was much less of a problem with PMMA and easier-to-bond materials. Only tests on high-density polyethylene material (HDPE) are presented in this report.

2.3. Position of gauges

Of particular interest was monitoring the strain as near as possible to the crack-initiation site and to relate this to forces monitored at the striker contact point by sensors in the striker. This should have regard for the yielding of the surface material around the crack tip and should also take into account that the fast crack propagation would mostly be influenced by the bulk properties of the specimen material. The position of strain gauge sensor found to be most suitable was $W/2$ (i.e. 20 mm) from the tip of the pre-crack along the length of the specimen, as shown in Fig. 1. The position of this site was not too critical and it fitted in well with the positioning of strain gauge sensors for other materials including metals [7].

Of course, once the crack was initiated, the strain as seen by this $W/2$ sensor would be affected by the redistribution of strain within the specimen. Another site that captured better the overall strain within the specimen, very similar to that seen by the striker sensor, was that placed in the compression zone of the specimen, this being situated on the same side of the specimen but nearer to the striker. Having regard for the surface effects, the sensor was placed $W/8$ from the impact edge of the specimen and $W/2$ away from the crack. This will now be referred to as the $W/2 \times W/8$ position.

To validate the positioning of the sensors, as well as exploring other adjacent sites, a duplicate set of gauges were secured on the opposite side of the pre-crack in the specimen. Good agreement was achieved and small errors in positioning of the gauges had an insignificant effect on the test results. For each specimen fitted with strain gauges, a preliminary load calibration was made to check the outputs from the strain gauge amplifiers. This was to check that the strains were reproducible for the same application of static loads. The specimen was placed into the same calibration fixture in the two possible orientations as a further check on the gauges and on any undue sensitivity to slight misalignments. Given that all these static tests were consistent, the gauge was finally calibrated in the static test rig just prior to impact loading of the specimen. Fig. 2 shows a calibration curve for a strain gauge $W/2$ from the tip of the pre-crack.

3. Results

3.1. Force-time traces

Fig. 3 shows a set of force-time test records obtained from fracturing a polyethylene (HDPE) specimen at room temperature using a falling mass of 65 kg to impact at a velocity of 5 m s^{-1} . The force-time trace (a) is from the sensor embedded in the striker and traces (b) and (c) are those from two strain gauges attached to the specimen on either side of the crack. This is at a distance along the length of the specimen of half of its width and aligned with the pre-crack tip which is at a half-way point through the specimen.

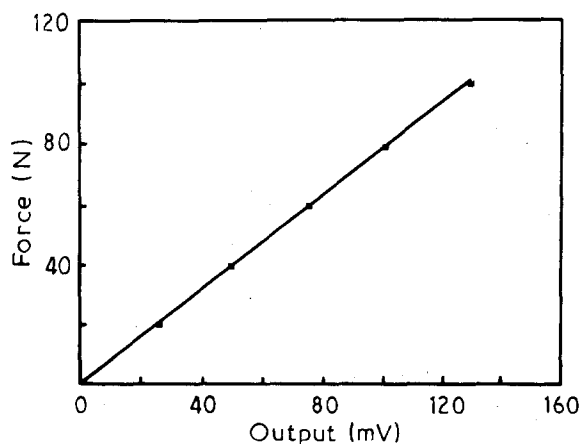


Figure 2 Calibration curve for $W/2 \times W/2$ on-specimen strain gauge as used in Fig. 3.

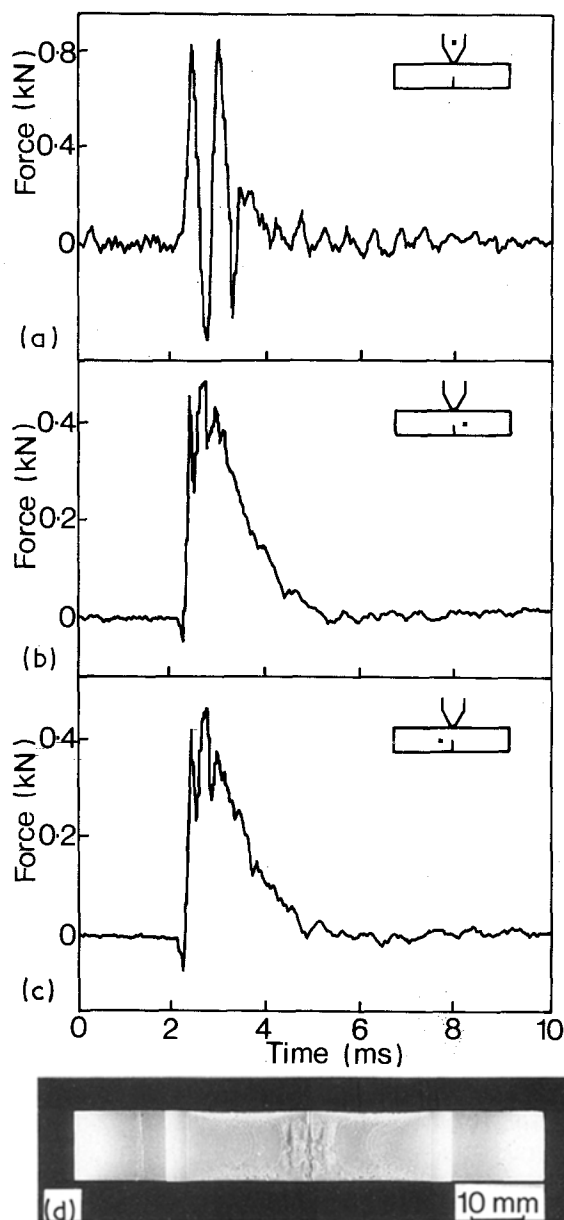


Figure 3 (a) Force-time trace from strain gauge sensor in the striker (impact velocity 5 m s^{-1} and specimen temperature 25°C); (b, c) force-time traces of on-specimen strain gauges in $W/2 \times W/2$ position; (d) optical photograph of fracture surface.

This will now be referred to as the $W/2 \times W/2$ position. As can be seen, the (b) and (c) sensors produced near-identical traces which confirms well the symmetry of strain distribution about the crack and the equal consistency in response of the sensors and monitoring channels. It is evident that the (b) and (c) sensors are in better positions than the striker sensor, at least to monitor the strain building up at the pre-crack tip to initiate the fracture crack and also to monitor at the crack site the impact transient excursions superimposed on the three-point bend strain at this time. Mostly, these observed transient excursions will be due to induced and reflected transverse wavefronts. A problem with the sensor in the striker is that as well as monitoring the overall force acting on the specimen, its output can also be more influenced by any reflections there may be in the striker and also by the striker to specimen contact conditions.

There can also be a loss of contact between striker and specimen and its two end supports [17]. The effect of loss of contact or bounce can be very important for some impact studies. In some cases, having force-time traces from sensors on the specimen and also from sensors in the striker and supports can be most helpful in resolving better very involved traces which tend to mask the point of failure of the specimen. Also, the force-time traces in Fig. 3 can greatly aid in the task of relating forces to crack initiation, fast crack propagation, tear lips and plastic hinges at the concluding root of the fracture.

Fig. 3d shows an optical micrograph of the fracture surfaces which show up well the fast crack, side tear-lips and plastic hinge zone. An observation is that there appears to be some correlation between the tear lips and arrest lines, but more information is needed to determine if this is a cause or effect of some other prime cause. This topic will be discussed again later.

Fig. 4 is a test result from a similar specimen with the same impact mass of 65 kg and impact velocity of 5 m s^{-1} . What has been changed is the location of one of the on-specimen sensor positions. One is still at the $W/2 \times W/2$ position and the other is moved over to the same side of the specimen with respect to the pre-crack and is also placed $W/2$ from the crack, but $W/8$ from the edge of the specimen. This is the edge with which the striker impacts so the $W/2 \times W/8$ positioned sensor is located in the compression zone when the specimen is subjected to a three-point bend. As the $W/2 \times W/8$ sensor is near to that in the striker then if there is firm contact between striker and specimen, both these sensors will tend to see the same forcing conditions. However, contact pressure between striker and specimen can and does change and this can be to include loss of contact or bounce. The $W/2 \times W/8$ sensor position can be very useful for helping to study these contact and bounce conditions and also for helping to observe the fall-off of the strain, as seen by the $W/2 \times W/2$ sensor, after crack initiation and whilst the crack is still propagating. Of course, there are different failure rates for the fast crack in the core of the material, the tearing of the side lips and the rupturing of the hinge bend material. By studying the three traces presented in Fig. 4, an indication is that the fast crack in the central core of the specimen is first to run out of the initiation zone followed by the tearing of the side-lips. The final phase is the failure of the hinge material although in some cases, this can survive the impact so that additional kinetic energy is absorbed by the specimen. This failure sequence is what may be expected, but it is how they overlap for different impact conditions that is of most interest.

A feature with the on-specimen strain gauge traces is that they often start off with a small excursion in one direction before recording the main trace in the opposite direction. This is discussed in the analysis section presented later.

Fig. 5 shows the results for fracturing a specimen at -20°C . The specimen is identical in all other ways to that used for the 25°C (Fig. 4) experiment. Also, the same impact mass of 65 kg was used impacting at 5 m s^{-1} . For the Fig. 5 experiment, only one on-

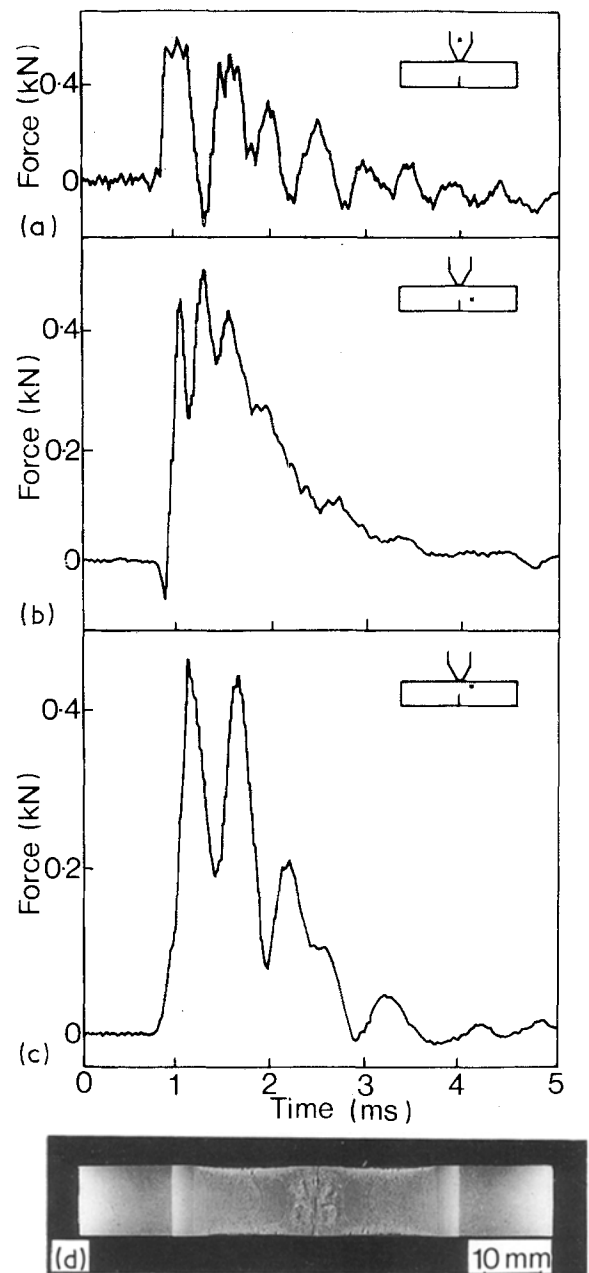


Figure 4 (a) Force-time trace from strain gauge sensor in the striker (impact velocity 5 m s^{-1} and specimen temperature 25°C); (b) force-time trace of on-specimen gauge in $W/2 \times W/2$ position; (c) force-time trace of on-specimen gauge in $W/2 \times W/8$ position; (d) optical photograph of fracture surface.

specimen sensor was used and this was in the $W/2 \times W/2$ position. As expected, the specimen material in its colder more brittle state failed earlier and the crack propagation was faster than for the 25°C tests. With the force-time curves in Fig. 5 is an optical photograph (Fig. 5c) of the fracture surface of the -20°C specimen. On comparing this fracture surface with that for the 25°C specimens, the difference in the size of the tear lips and hinge section should be noted. Also of interest, is a comparison of the prominence and different position of the fast crack arrest lines.

Figs 6 and 7 give the results of another pair of experiments with specimens at 25 and -20°C . In this case, the specimens were identical to those used before and with sensors at the $W/2 \times W/2$ and $W/2 \times W/8$ positions. The impact velocity of the 65 kg mass in this case was 2 m s^{-1} . As expected with a lower impact

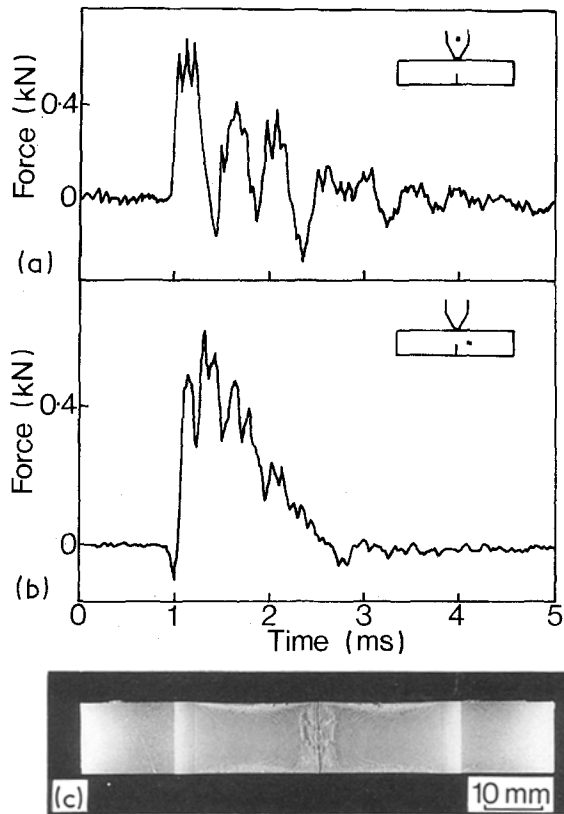


Figure 5 (a) Force-time trace from strain gauge sensor in the striker (impact velocity 5 ms^{-1} and specimen temperature -20°C); (b) force-time trace of on-specimen strain gauge in $W/2 \times W/2$ position; (c) optical photograph of fracture surface.

velocity, the transient excursions on the force-time curves are less strong. Also, it took longer to fracture the specimens at this lower impact velocity. Not presented in this sequence of experiments are the results of impacts at velocities greater than 5 ms^{-1} when there can be significant bounce at the contact point between striker to specimen and specimen to support points. Mostly, this is because for these higher velocity experiments different positioning of on-specimen sensors needs to be found. Also, more than two sensors and instrument channels are required for best results and these were not available at the time of this study. However, information on bounce effects from another research programme is given in [17].

Fig. 8 shows the results of the next step in this research sequence which was to side-groove the specimen either side of the crack path in order to eliminate, as much as possible, the effect of side shear-lips. A side-grooved specimen at 25°C was then subjected to impact by the 65 kg mass at a velocity of 5 ms^{-1} . Very noticeable when comparing these results with those for specimens without side-grooves is that whilst the force and time of the fast crack initiation is very similar, the time to fracture fully a specimen is much less for the side-grooved specimens. In view of the earlier comment in this paper about the possible link between side tear-lips and arrest lines in the fast crack surface, it is interesting to note that the arrest lines in the fast crack surfaces (see Fig. 8d) of the side-grooved specimens are quite faint.

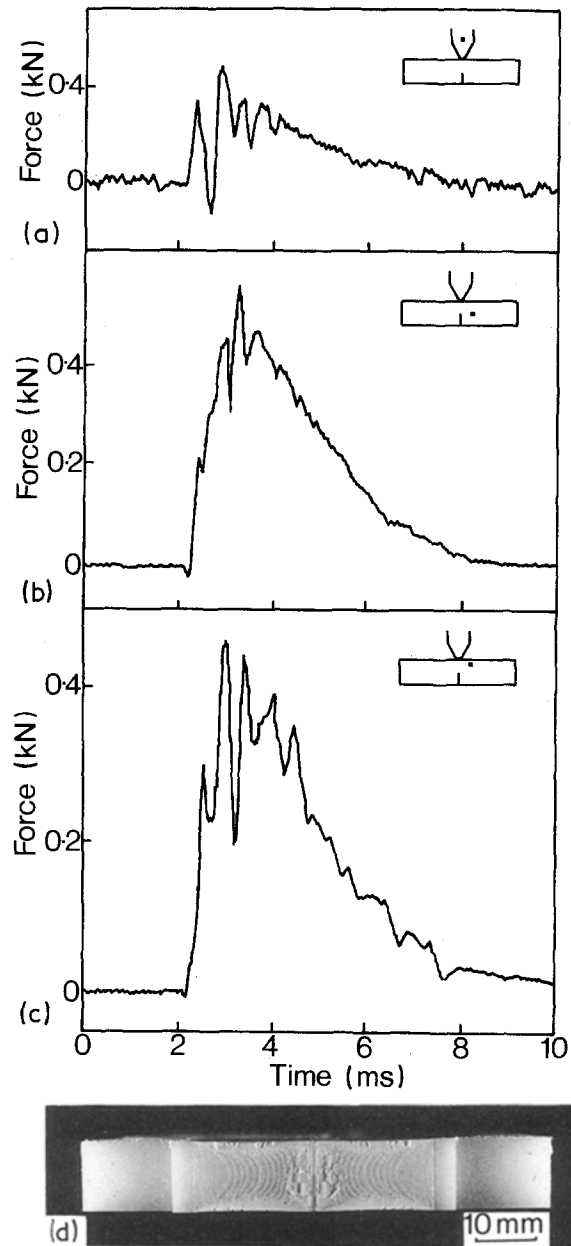


Figure 6 (a) Force-time trace from strain gauge sensor in the striker (impact velocity 2 ms^{-1} and specimen temperature 25°C); (b) force-time trace of on-specimen gauge in $W/2 \times W/2$ position; (c) force-time trace of on-specimen gauge in $W/2 \times W/8$ position; (d) optical photograph of fracture surface.

3.2 High-speed photography

To help in the study and analysis of crack and other failure processes in materials under test, high-speed photographic techniques can be used to capture more information than is possible by other means. For the work reported here, two photographic studies (see Fig. 9a and b) were made to observe crack propagation, one being for a specimen tested at room temperature at an impact velocity of 5 ms^{-1} without side-grooves and the other for a specimen with side-grooves. In the former case, of course, what is seen is the well-rounded cleavage point of the tear-lip following on behind the hidden fast crack in the core of the specimen. Comparing the two photographic sequences, without and with side-grooves, provides some information on the effect of tear-lips in the specimen. With side-grooves, the crack visible in the high-speed photographs

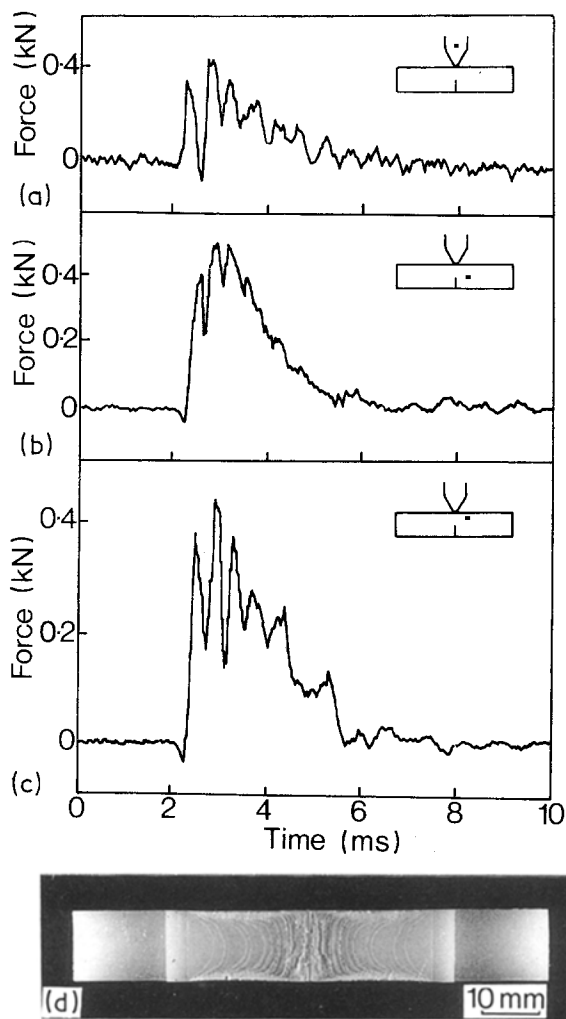


Figure 7 (a) Force-time trace from strain gauge sensor in the striker (impact velocity 2 ms^{-1} and specimen temperature -20°C); (b) force-time trace of on-specimen strain gauge in $W/2 \times W/2$ position; (d) optical photograph of fracture surface.

(Fig. 9b) can be taken as the fast crack. Without side-grooves, the crack seen by the camera is the side-lip tearing (Fig. 9a). An interesting point when comparing the photographs of specimens with and without side-grooves is that the fast crack in both specimens seems to have been initiated at very much the same overall strain of the specimen and it may well be that the fast crack velocity in both tests is similar but this needs further verification. In the case of the specimen without side-grooves (Fig. 9a), the photographic sequence has captured well the initial fork-like depression, labelled F, of the tear-lip crack and how this changes to a well-radiused blunt crack-tip as the tear-crack traverses the specimen. To observe this effect, a single illuminating light source was set to one side so that the surface depression of the yielding material around the tear-lips would create a shadow. This, of course, meant that the overall lighting of the specimen was not even. However, the rollers supporting the end of the specimen can be seen and because of the lighting, these throw a shadow on to the specimen. The top of the striker shows up as a bright line because its upper surface is cylindrical.

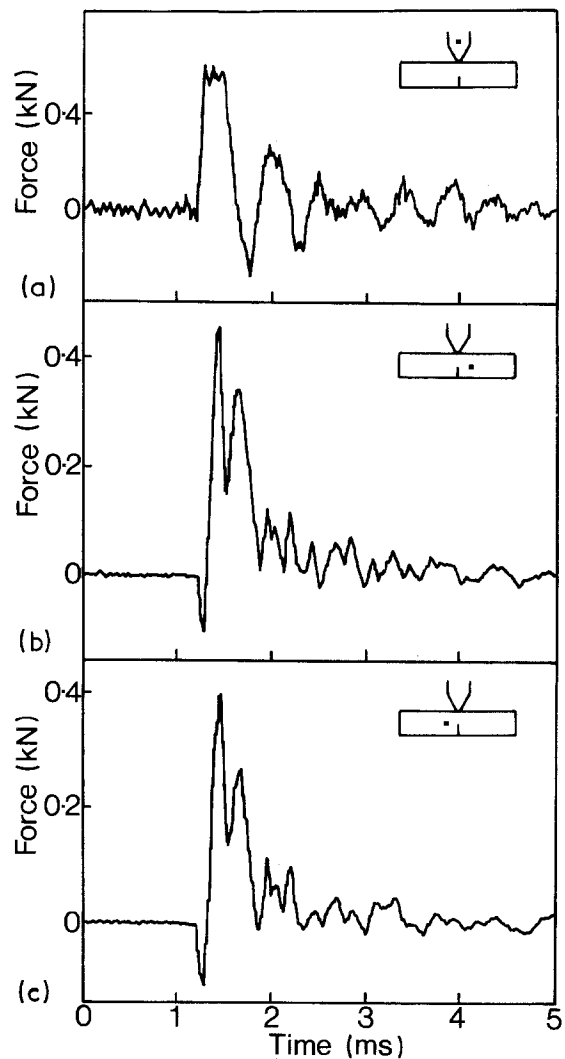


Figure 8 (a) Force-time trace from strain gauge sensor in the striker for a side-grooved specimen (impact velocity 5 ms^{-1} and specimen temperature 25°C); (b, c) force-time traces of on-specimen strain gauges in $W/2 \times W/2$ position; (d) optical photograph of fracture surface.

4. Analysis

The experiments in this paper were devised to achieve a good measurement of fracture toughness, K_{Ic} , and fracture energy, G_c , for the impact velocities used. This is to provide for some interesting comparisons to be made. In particular, for specimens with $S/W = 4$, as employed in these experiments, the following expression was used to determine the fracture toughness, K_{Ic} [19]

$$K_{Ic} = (6P_c Y a^{1/2}) / (BW) \quad (1)$$

where P_c is the peak load at crack initiation, a is the length of the sharp pre-crack, B is the thickness, W is the width of the specimen and Y is a dimensionless geometry factor which is given by

$$Y = \frac{\{1.99 - a/W(1 - a/W)[2.15 - 3.93a/W + 2.7(a/W)^2]\}}{(1 + 2a/W)(1 - a/W)^{3/2}} \quad (2)$$

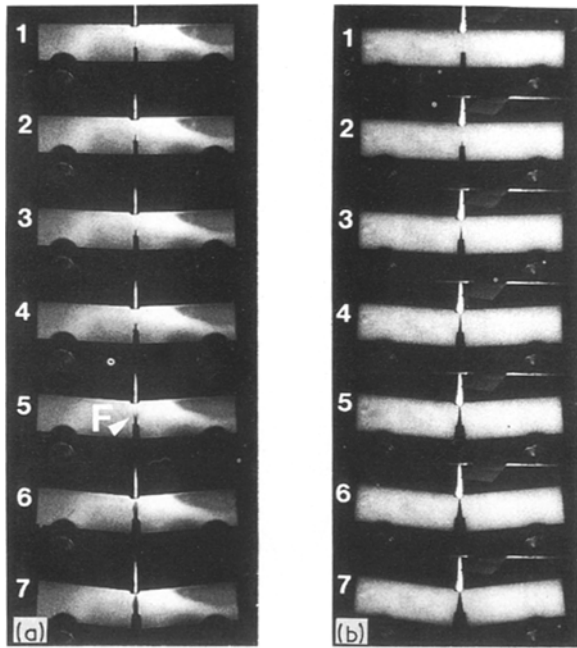


Figure 9 High-speed photographic sequences (Interframe time 0.25 ms) of impact at 5 m s^{-1} of specimens at temperature 25°C : (a) without side-grooves, (b) with side-grooves.

Using a LEFM analysis [4], the fracture energy, G_c , is given by

$$G_c = \frac{P_c^2 dC}{2B da} \quad (3)$$

where C is the compliance of the test specimen (i.e. displacement/load). Introducing a dimensionless geometry factor, ϕ [20], given by

$$\phi = \frac{C}{dC/d(a/W)} \quad (4)$$

G_c can be calculated using [4]

$$G_c = U_c/(BW\phi) \quad (5)$$

where U_c is the stored elastic strain energy in the specimen at crack initiation.

One of the main purposes of this research was to make comparisons between K_{Ic} and G_c as determined using strain gauge data obtained from a sensor on the striker and from sensors located on the specimen. The difference between the two sets of derived K_{Ic} and G_c is mainly due to the dynamic behaviour of the specimen as excited by the impact transient forces. This is to include bounce by the specimen at the striker and support points, as well as the vibration excursions of the specimen. An important point is that the on-specimen strain gauges will more closely monitor the strain near to the crack tip. It was necessary to obtain from other research [21] the relationship between static loading and dynamic loading at 5 and 2 m s^{-1} of the HDPE specimens for temperatures of 25° and -20°C and to apply these calibration factors to the experimental measurements recorded in this study. A difficulty when determining G_c was to be precise about the energy absorbed by the specimen up to the crack initiation point in the impact test because of the transient swings superimposed on the force–time

traces. In the case of the striker sensor, it monitored the force as applied to the specimen as a whole. Some of the energy under the force–displacement curve could be absorbed as kinetic energy by the fractured parts of the specimens, whereas the sensors on the specimen near to the crack tip would be monitoring more closely the smaller amount of strain energy which is available to propagate the crack. It follows that G_c , as derived using the striker sensor, would be higher than that using the on-specimen sensors. For this work, the area under the force–displacement curve up to the onset of crack propagation was taken as a good estimate of the energy available for crack initiation. This is both for the force–time traces from the sensor on the striker and those on the specimen.

For ease of comparison, several sets of numerical data are given in Table I. Also presented are the time to initiate crack propagation (t_i) and the time to sever fully the specimen (t_f). An interesting point is that the fast crack propagation in the central core of the specimen is at a rate of $\sim 50 \text{ m s}^{-1}$ (time for fast crack to propagate is $\sim 0.4 \text{ ms}$). It is thought that the fast crack in the material without side-grooves will be close to the 50 m s^{-1} figure, and the forces then acting on the specimen are those tearing the side-lips. Taking into account the geometry of the specimen as it fractures, clearly the tear-lip material puts up a surprisingly high resistance to being fractured, as shown in the force–time diagrams (Figs 3–7). As expected, the values of K_{Ic} and G_c are more consistent for experiments at room temperature than for those when the specimens were cooled to -20°C . This is partly, because of the handling of the cold specimens and the differing times taken to do the impact test. In making the above calculations for K_{Ic} and G_c , both strain gauge force–time traces have been used from sensors in the $W/2 \times W/2$ position and sensors in the $W/2 \times W/8$ position. This is valid because the early part of the force–time curve up to the initiation of fast crack propagation represents well the overall strain in the specimen. However, once the crack starts to extend, the strain within the specimen is redistributed so as to reduce that experienced by the $W/2 \times W/2$ gauge.

A reason for deciding upon the chosen size of sample and conditions for impact test was so that better information about the fast crack propagation in the core of the specimen, the tear lips and the hinge failure could be obtained. Fig. 10 shows electron micrographs at the same magnification of these different regions of the fracture surface. Notable is the much finer micro-ductility of the fast crack surface in the core of the specimen compared with that of the tear lip and the hinge failure surfaces. This is for impact conditions when the failure occurs amidst early strong transient excursions of the striker force–time trace. The values of K_{Ic} and G_c in Table I are evaluated using the first peak of the strain gauge force–time curves. Of particular interest is that K_{Ic} and G_c values for specimens with and without side-grooves are very similar. This confirms the point made above that the initiation and fast crack propagation can dominate the early failure of the specimen. It is after the fast crack has propagated that the side-lip tearing and hinge failure

TABLE I For different striker impact velocities and specimen temperatures, the tabulation gives calculated values of K_c (critical stress intensity factor) and G_c (critical strain energy release rate)

Impact velocity ($m s^{-1}$)	Temp. ($^{\circ}C$)	t_i (ms)	P_e^{sg} (kN)	P_e^{st} (kN)	K_c^{sg} ($MPa m^{1/2}$)	K_c^{st} ($MPa m^{1/2}$)	G_c^{sg} ($kJ m^{-2}$)	G_c^{st} ($kJ m^{-2}$)	t_f (ms)
5 (Fig. 3)	25	0.210 ($W/2 \times W/2$)	0.449	0.823	2.1	3.9	2.1	4.8	3.0
			0.416		2.0		1.9		
5 (Fig. 4)	25	0.228 ($W/2 \times W/2$)	0.452	0.603	2.1	2.8	2.0	4.6	3.0
			0.466		2.2		2.1		
5 (Fig. 5)	-20	0.168 ($W/2 \times W/2$)	0.491	0.686	2.3	3.2	1.7	4.3	1.7
2 (Fig. 6)	25	0.900 ($W/2 \times W/2$)	0.445	0.494	2.1	2.3	2.7	3.8	6.0
			0.445		2.1		2.6		
2 (Fig. 7)	-20	0.436 ($W/2 \times W/2$)	0.407	0.440	1.9	2.1	1.7	2.8	3.5
			0.384		1.8		1.7		
5 (Fig. 8)	25	0.240 ($W/2 \times W/2$)	0.449	0.603	2.1	2.8	1.9	4.5	0.65
			0.395		1.9		1.7		

P_e is the peak load to initiate crack propagation, t_i is the time to initiate crack propagation at load P_e , t_f is the time to sever fully a specimen, P_e^{sg} is the peak load measured from strain gauge output, and P_e^{st} is the peak load measured from striker output.

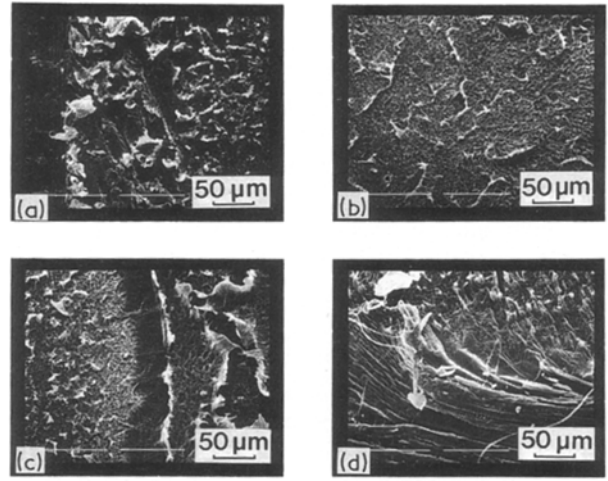


Figure 10 Electron micrographs of (a) the crack initiation zone, (b) fast crack failure surface in core of specimen, (c) the hinge failure surface, and (d) the tear-lip failure surface.

significantly affect the continuing failure processes as revealed by the force-time traces.

The values of K_c and G_c derived from the on-specimen sensors (K_c^{sg} and G_c^{sg}) have much less scatter than K_c and G_c values derived from the force-time traces of the striker sensor (K_c^{st} and G_c^{st}). Generally, it is easier to identify more precisely the peak load and the time that failure is initiated in the specimen when using an on-specimen sensor. This can be seen by inspection of the traces in Figs 3–8. The higher the impact velocity, then the stronger and more erratic are the oscillatory excursions and the shorter is the time to failure. It is for these higher impact velocities of the striker that the on-specimen sensors are particularly useful for helping to analyse test results, and also for calibrating the striker sensor which is then used for routine tests.

Looking in more detail at the reasons for uncertainty in determining the peak load and the elastic energy stored in the specimen prior to its failure, the following factors are relevant. It follows that the higher the impact velocity of the striker then the greater will be the effect of the initial transient forces on the failure test results. One feature can be that the specimen zone near to the impact site can be significantly deformed by the first contact effects of the impact. This is before the specimen as a whole is taken into a three-point bending configuration. The on-specimen sensors near to the crack site will see the stresses created by this early impact deformation of the specimen. In the case of the tests reported in this paper, it is to be noted that the force-time traces for the on-specimen sensors near to the crack tip first dip before following the build up of three-point bending load in the specimen. This is because the sensors experience the early impact stresses. Of course, depending on where the on-specimen sensors are located, observation of the early impact stresses can be different and this is a very useful way of analysing these effects.

As mentioned above, for a polyethylene specimen of given dimensions, it is difficult to make comparisons between static and dynamic failure of the specimen.

This is mainly due to crack-tip blunting and other processes which occur at low loading rates. It is possible to use very thick specimens in static tests to achieve a more brittle failure or, of course, the specimen can be cooled to low temperatures. Clearly, in such cases when changing a number of test conditions, misleading indications can be obtained. In this case, the main interest was the dynamic performance of specimens of the size used, and research elsewhere [4] has examined the static and dynamic relationships of polymer materials.

However, the indications in Table I are quite clear that both K_c and G_c are generally higher when using the output from the striker sensor than when using the output from the on-specimen sensors. A main factor is that the forces seen by the striker sensor relate to those acting on the specimen as a whole, not only to initiate fracture but also to generate dynamic vibrations and to impart kinetic energy to the fractured specimen parts whereas the on-specimen sensors tend to see mostly the strain caused by forces focused on to the crack site. There is also the additional point that the transient excursions are less in evidence in the on-specimen sensor traces than those for the striker sensor. This is particularly noticeable for the $W/2 \times W/2$ sensor. A further point which is examined more fully in [17] is that under strong transient conditions, such as are in evidence in the research reported here, there is the question as to the true quantity of stored energy available in the strained specimen at the point of failure and the extent to which this can flow into the crack site and generate a crack surface. However, for this research the main requirement was the ability to compare the pre-crack energy stored in the specimen as measured by using the striker sensor, and the specimen sensor.

5. Conclusions

As advances in materials are made and there is wider use of composite structures of many different kinds, so there is increasing interest in the strain distribution within a specimen, when subject to impact loading up to and including its failure. As a basis for more research into the area, this paper reports the transient strain patterns generated in homogeneous specimen materials as monitored by on-specimen strain gauges. With suitable multi-channel monitoring systems, the work reported here indicates that comprehensive studies can effectively be made. With some materials such as polyethylene studied in this paper, observing the surface of the material using laser speckle, holography and such techniques, may not reveal very well the forces acting on the core of the material because of surface yield effects. However, when used in parallel with the type of experimentation covered in this paper, there is much to be learnt about the behaviour of materials under impact loading and very much so for the stress transfer properties for materials having an oriented chain as well as those having composite structures. A key point is that whatever material or composite is being considered, there will be a difference in the forces experienced by the striker sensor and

those experienced by the on-specimen sensors. This is not only important from the point of view of obtaining more precise information on the build up of strain at the crack tip and so obtaining more realistic values for K_c , G_c and other fracture mechanics parameters, but also the difference between striker and on-specimen sensor measurements can be of great value to a designer. This is very much so when the specimen represents more closely a working structure. An important design consideration is to reduce the concentration and level of stress at likely failure points. It is thought that there is a great deal of research needed in this area that will require painstaking attention to experimental detail in order to achieve worthwhile and well-validated results. It is hoped that this paper has made a contribution to this important area of research.

Acknowledgements

The authors thank Professor J. G. Williams for his interest and helpful discussion on this work and one of us (JPD) thanks BP Chemicals Ltd, for interest and support.

References

1. J. C. RADON and C. E. TURNER, *J. Engng Fracture Mech.* **1** (1969) 411.
2. W. L. SERVER and A. S. TETELMAN, *Engng Fracture Mech.* **4** (1972) 367.
3. T. KOBAYASHI, I. YANAMOTO and M. NIINONIMI, *ibid.* **24** (1986) 773.
4. J. G. WILLIAMS, "Fracture Mechanics of Polymers" (Ellis Horwood, Chichester, 1984) p. 237.
5. *Idem.*, *Int. J. Fracture* **33** (1987) 47.
6. J. H. MacGILLIVRAY, E. R. AKUM, P. BROOKS-JOHNSON and V. GRABULOV, in "Proceedings BSSM/SEM International Conference on Advanced Measuring Techniques", London, edited by K. Whittles (Whittles, Latheronwheel, Scotland, 1987).
7. J. H. MacGILLIVRAY, DTI Final Report, March (1989).
8. J. G. WILLIAMS and G. C. ADAMS, *Int. J. Frac.* **33** (1987) 209.
9. J. P. DEAR and J. E. FIELD, *J. Appl. Phys.* **65** (1988) 533.
10. J. P. DEAR, J. E. FIELD and A. J. WALTON, *Nature* **332** (1988) 505.
11. J. E. FIELD, M. B. LESSER and J. P. DEAR, *Proc. R. Soc. London Ser. A* **53** (1985) 101.
12. J. P. DEAR and J. E. FIELD, in "Proceedings of the 7th International Conference on Erosion by Liquid and Solid Impact", edited by J. E. Field and J. P. Dear (Cavendish Laboratory, Cambridge, UK, 1987) paper 3.
13. A. J. KINLOCH, G. A. KODOKIAN and M. B. JAMARANI, *J. Mater. Sci.* **22** (1987) 4111.
14. J. F. KALTHOFF, *Int. J. Frac.* **27** (1985) 277.
15. B. A. CROUCH and J. G. WILLIAMS, *J. Mech. Phys. Solids* **36** (1988) 1.
16. W. BÖHME and J. F. KALTHOFF, *Int. J. Fracture* **20** (1982) 139.
17. J. P. DEAR, *J. Appl. Phys.* **67**(9) (1990) 4304.
18. M. K. V. CHAN and J. G. WILLIAMS, *Int. J. Fracture* **23** (1983) 145.
19. J. E. STRAWLEY, *ibid.* **12** (1976) 475.
20. E. PLATI and J. G. WILLIAMS, *Polym. Engng Sci.* **15** (1975) 470.
21. W. CHUNG, PhD Thesis, Imperial College, University of London (1989).

Received 25 October 1989
and accepted 20 April 1990